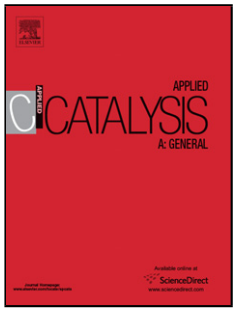

Title: Promoter effect of sodium in graphene-supported Ni and Ni-CeO_2 catalyst for the low-temperature WGS reaction

Author: A.B. Dongil L. Pastor-Pérez A. Sepúlveda-Escribano P. Reyes

PII: S0926-860X(15)30088-0
DOI: http://dx.doi.org/doi:10.1016/j.apcata.2015.07.036
Reference: APCATA 15486

To appear in: *Applied Catalysis A: General*

Received date: 27-4-2015
Revised date: 7-7-2015
Accepted date: 23-7-2015

Please cite this article as: A.B.Dongil, L.Pastor-Pérez, A.Sepúlveda-Escribano, P.Reyes, Promoter effect of sodium in graphene-supported Ni and Ni-CeO2 catalyst for the low-temperature WGS reaction, Applied Catalysis A, General http://dx.doi.org/10.1016/j.apcata.2015.07.036

Promoter effect of sodium in graphene-supported Ni and Ni-CeO_2 catalyst for the low-temperature WGS reaction

A. B. Dongil[a], L. Pastor-Pérez[b], A. Sepúlveda-Escribano[*b], P. Reyes[a]

[a] *Universidad de Concepción, departamento de físicoquímica, laboratorio de catálisis por metales, Edmundo Larenas 129, Concepción, Chile.*

[b]*Laboratorio de Materiales Avanzados, Departamento de Química Inorgánica - Instituto Universitario de Materiales de Alicante, Universidad de Alicante, Apartado 99, E-03080 Alicante, Spain*

(*) corresponding author: asepul@ua.es

Graphical abstract

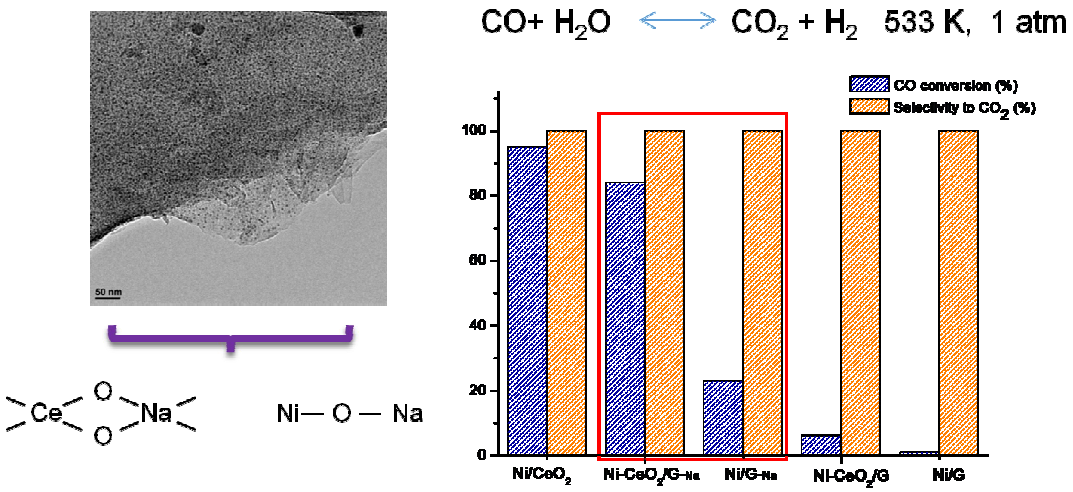

Highlights

- Graphene-supported Ni and Ni-CeO_2 catalysts have been studied.
- Metal dispersion depends on the presence of ceria and on the precipitating agent, NaOH or urea.
- The graphene support strongly interacts with the ceria promoter.
- The presence of sodium increases the catalytic activity, mainly in the presence of ceria.

Abstract

The low temperature water-gas shift (WGS) reaction has been studied over Ni-CeO_2/Graphene and Ni/Graphene. The catalysts were prepared with 5 wt% Ni and 20 wt% CeO_2 loadings, by deposition-precipitation employing sodium hydroxide and urea as precipitating agents. The materials were characterized by TEM, powder X-ray diffraction, Raman spectroscopy, H_2-temperature-programmed reduction and X-ray photoelectron spectroscopy (XPS). The characterization and the reaction results indicated that the interaction between the active species and the support is higher than with activated carbon, and this hinders the reducibility of ceria and thus the catalytic performance. On the other hand, the presence of residual sodium in samples prepared by precipitation with NaOH facilitated the reduction of ceria. The catalytic activity was highly improved in the presence of sodium, what can be explained on the basis of an associative reaction mechanism which is favored over Ni-O-Na entities.

Keywords: Graphene; Ni; Na doping; Ceria; Water-gas shift.

1. Introduction

The water-gas shift reaction (WGS, CO + H_2O → CO_2 + H_2) has gained increased attention in the last years due to its importance in the production and purification of hydrogen from fossil and renewable resources. It can be coupled at the exit of a reforming unit to obtain a high purity hydrogen stream which can be used to feed fuel cells [1]. Metal/ceria systems have been proved to offer excellent performance for the low temperature stage of WGS [2], Pt/ceria being the most promising catalyst in terms of activity and selectivity [3,4]. The ability of CeO_2 for the $Ce^{+4} + e^- \leftrightarrow Ce^{+3}$ redox process and the formation of oxygen vacancies favour the mobility of surface oxygen species [5], which are active in the reaction. Furthermore, a synergistic effect is obtained between metal and ceria. On one hand, ceria reducibility is favoured when the metal is in close contact with its surface and, on the other hand, ceria can stabilize the metal nanoparticles avoiding their agglomeration [6]. However, given the low availability of ceria, it is interesting to optimize its use, for example by spreading it onto a high surface area support. In this sense, we have reported in previous papers the promoter effect of ceria in activated carbon-supported Pt catalysts, where the interaction between the metal and the oxide is enhanced [7]. Another challenge in the developing of a WGS catalyst is the replacement of platinum by a more economical metal.In this sense, nickel has been the metal of choice for certain reforming reactions due to its competitive price, high availability and activity [8,9], and it has proved to be active and selective in the WGS reaction when it is highly dispersed [10,11].

An excellent metal dispersion and an optimal metal-ceria interaction are therefore mandatory to achieve an optimal catalytic performance. In this scenario,

graphite oxide (GO) emerges as an excellent candidate to act both as substrate for the synthesis of supported nanoparticles and as precursor of the support. GO displays a rich oxygen chemistry, which allows its dispersion in aqueous solutions and the interaction with the metal and/or oxide precursors that would improve their dispersion. Several studies can be found concerning the use of GO as support [12], catalyst by its own [13,14]and as precursor of graphene (G) or reduced graphene oxide (rGO) [15]. For this latter approach, both metal/G or metal/rGO [16,17] and metal/oxide/G or metal/oxide/rGO systems [18,19,20] have also been developed. The synthesis of the metal and oxide nanoparticles can be performed before its deposition on the support, for example by colloidal methods [19], or simultaneously to the synthesis of graphene [18]. The resulting material provides good nanoparticle dispersion with homogeneous distribution [21]. In some cases, it has been suggested that additional improvement on the catalytic performances, due to a synergism between GO and the active phase, was achieved [22]. Depending on the metal, the synthesis of the nanoparticles can be performed under mild conditions, as is the case for Ag [19], or may require the use of stronger reducing agents [17,20].

In this work we have performed the synthesis of the binary Ni/Graphene and the ternary Ni-CeO_2/Graphene systemsemploying urea and sodium hydroxide as precipitating agents for depositing the active phases on the graphene support. The catalysts have been thoroughly characterized and their catalytic performance has been tested in the low temperature stage of the WGS reaction.

2. Experimental section

2.1. Synthesis of graphite oxide

Graphite oxide (GO) was prepared from natural flake graphite according to a modified Hummers method [23]. Briefly, 3 g of natural graphite powder was added to a reaction flask containing concentrated H_2SO_4 (25 $mL \cdot g^{-1}$ of support) and 1.5 g of sodium nitrate, which was previously cooled to 273 K in an ice bath. Then, potassium permanganate (9 g) was slowly added and kept under stirring at 298 K for 30 min. Then, 138 mL of deionized (DI) water was slowly added and the suspension was maintained at 373 K for 15 min. Finally, 420 mL of deionized water was added, followed by the slow addition of 30 mL of hydrogen peroxide. The suspension was filtered off and washed extensively with deionized H_2O, HCl (30%) and ethanol, and finally dried in vacuum at 333 K for 24 h to obtain the graphite oxide (GO) powder, which was kept in a desiccator until use.

2.2. Catalyst synthesis

For the synthesis of the catalysts, GO was dispersed in deionized water (1 $mg \cdot mL^{-1}$) and sonicated for 30 min. The required amount of $Ce(NO_3)_3 \cdot 6H_2O$ (99.99%, Sigma–Aldrich) to obtain a 20 wt.% CeO_2 was dissolved in 10 mL of DI water and added dropwise to the GO dispersion with stirring. The resulting slurry was stirred for 2.5 h. Then, the necessary amount of $Ni(NO_3)_2 \cdot 6H_2O$ (99.9%, Sigma–Aldrich) to obtain a 5 wt.% Ni loading was dissolved in 10 mL of DI water, added dropwise to the mixture and stirred for 2 h. Aqueous 0.5 M solutions of NaOH or urea were used as precipitating agents. The addition of the NaOH solution was carried out dropwise, with stirring. When urea was used, the solution was mixed with the GO suspension containing the nickel and the ceria precursors, and the resulting slurry was heated at 363 K, with stirring, to reach a pH of around 11. In both cases, the formed slurries were stirred for 2 h and, after

cooling to room temperature, the solid was filtered off, washed extensively with water and ethanol, and finally dried at 313 K under vacuum for 24 h. The same procedure was applied for the catalyst with no ceria, using only a solution with the nickel precursor. Finally, the solids were heat-treated during 5 h at 623 K under flowing He (50 mL·min-1), with a heating rate of 1 $K \cdot min^{-1}$. The resulting materials were labelled as Ni-CeO_2/G-Na and Ni/G-Na for the catalysts prepared with NaOH, and Ni-CeO_2/G and Ni/G when the precipitating agent used was urea. For the sake of comparison, a Ni/CeO_2 catalyst was also prepared with 5 wt%. Ni loading. The ceria support was prepared by homogeneous precipitation from an aqueous solution of $Ce(NO_3)_3 \cdot 6H_2O$ (99.99%, Sigma–Aldrich) containing an excess of urea. The solution was heated at 353 K and kept at this temperature, with slow stirring, during 12 h. The solid formed was filtered and calcined at 623 K for 4 h. The CeO_2 support prepared in this way was impregnated with a solution of the nickel precursor in acetone. The excess of solvent was removed by vacuum treatment in a rotary evaporator.

2.3 Characterization

Conventional TEM analysis was carried out with a JOEL model JEM-210 electron microscope working at 200 kV and equipped with an INCA Energy TEM 100 analytical system and a SIS MegaView II camera. Samples for analysis were suspended in methanol and placed on copper grids with a holey-carbon film support.

X-ray powder diffraction patterns were recorded on a JSO Debye-flex 2002 system, from Seifert, fitted with a Cu cathode and a Ni filter, using a $2^{\circ} \cdot min^{-1}$ scanning rate.

Raman spectra were carried out at room temperature using a DXR Raman microscope with 532 nm excitation source from an Ar^+ laser.

Temperature-programmed reduction (TPR) with H_2 measurements were carried out with the heat-treated catalysts in a U-shaped quartz cell using a 5% H_2/He gas flow of 50 mL·min^{-1}, with a heating rate of 10 K·min^{-1}. Samples were treated with flowing He at 423 K for 1 h before the TPR run. Hydrogen consumption was followed by on-line mass spectrometry (Pfeiffer, OmniStar GSD 301).

Infrared spectra were collected by using a Nicolet Nexus spectrometer and recorded by a DTGS detector from 128 scans and with a resolution of 4 cm^{-1}. The samples were mixed with pre-dried potassium bromide to a final concentration of approximately 1 wt%.

X-Ray photoelectron spectroscopy (XPS) analyses were performed with a VG-MicrotechMultilab 3000 spectrometer equipped with a hemispherical electron analyser and a Mg-Kα (h = 1253.6 eV; 1 eV = 1.6302·10-19 J) 300-W X-ray source. The powder samples were pressed into small Inox cylinders. The catalysts were reduced *ex-situ* (H_2, 623 K, 1 h) and then introduced in octane under inert atmosphere. Suspensions were evaporated in the XPS system under vacuum conditions.Before recording the spectra, the samples were maintained in the analysis chamber until a residual pressure of ca. 5·10−7 N·m^{-2} was reached. The spectra were collected at pass energy of 50 eV. The intensities were estimated by calculating the integral of each peak, after subtracting the S-shaped background, and by fitting the experimental curve to a combination of Lorentzian (30%) and Gaussian (70%) lines. The binding energy (BE) of the C l s peak of the support at

284.6 eV was taken as an internal standard. The accuracy of the BE values is ± 0.2 eV.

2.4 Water-gas shift reaction

The catalytic behaviour of the prepared samples in the low temperature water–gas shift reaction was evaluated in a fixed bed flow reactor under atmospheric pressure in a range of temperatures from 413 K to 563 K. The feed gas stream contained a volume composition of 1.87% CO, 35.92% H_2O, and He balance, with a total flow of 100 mL·min-1. Activity tests were performed using 0.150 g of catalyst diluted with SiC, at a volume ratio of 1:2, to avoid thermal effects. Prior to the reaction, catalysts were reduced during 1 h at 623 K with flowing H_2 (50 $mL \cdot min^{-1}$). Reaction at each temperature was stabilized for 2 h, and the composition of the gas stream exiting the reactor was determined by on-line mass spectrometry (Pfeiffer, OmniStar GSD 301). The catalytic activity will be expressed by the degree of CO conversion.

3. Results and discussion

3.1 Characterization

Representative TEM images of the reduced catalysts (H_2, 623 K, 1h) are shown in Fig. 1. In general, samples presented wrinkled layers as well as some transparent areas corresponding to exfoliated graphene sheets. Some amorphous carbon was also present on the samples, though the Ni/G-Na material seemed to display a higher proportion. The images showed that Ni and/or NiO nanoparticles decorated the surface of the catalysts; however, the particle size distribution differed among the samples. Thus, for the Ni/G-Na catalyst a heterogeneous

distribution and nanoparticles as small as 3 nm could be observed, along with some large particles of around 20 nm, the estimated mean particle size being 10 nm. On the contrary, the Ni/G catalyst displayed a more homogeneous particle size distribution, as the representative image in Fig 1.b shows, with an estimated mean particle size of 5 nm. On the other hand, the images of Ni-CeO_2/G-Na showed well-dispersed nanoparticles throughout the sheets, and extended surface areas were covered. The size of these nanoparticles is in the range 2-3 nm, similar to values found in literature for the Ag/GO/CeO_2 system in which the synthesis was performed in the presence of a stabilizing agent[18]. On the other hand, the micrographs of the Ni-CeO_2/G catalyst showed agglomerated nanoparticles, and ceria crystallites could be clearly distinguished in some areas (Fig. S1).

The X-ray diffraction patterns of the parent supports and the calcined catalysts are shown in Fig. 2. The diffractogram obtained with GO presented a well-defined peak at 10.6º corresponding to the (001) reflection of graphite oxide, and it can be observed that the peak at $2\theta = 26º$ corresponding to the (002) reflection of graphite decreased significantly, this proving a high yield in the synthesis. The interlayer distance given by the Bragg´s equation, 0.83 nm, is in the range of the values normally obtained with this method of synthesis [23,24]. For the Ni/G-Na and Ni/G catalysts the diffraction peak at 10.6º disappeared, this indicating the reduction of the parent GO, and the XRD patterns displayed the diffraction peak at 26º that corresponds to the (002) reflection of graphite, although their wideness suggest that the structure is different to that of the parent graphite. Additionally, a shoulder at 22º is insinuated in the XRD pattern of both samples, which can be ascribed to turbostratic graphite [25]. For catalyst Ni/G-Na, a diffraction peak at around 44º can be observed, which might include the (400) reflection of NiO

[16]along with the (100) reflection of graphite. This would be in agreement with the larger particles shown in TEM analysis (Fig. 1). When ceria was present in the catalysts the peak ascribed to GO also disappeared, but the XRD patterns were different from those obtained for Ni/G-Na and Ni/G. The XRD pattern of Ni-CeO_2/G showed four well defined peaks at 28.6º, 33.7º, 47.6º and 56.5º, which correspond to the reflections in the (111), (200), (220) and (331) crystalline planes of the cubic fluorite-type phase of ceria, along with the reflection of the (002) plane of graphite at 26º. On the other hand, the XRD pattern of Ni-CeO_2/G-Na showed the same reflections, although they appeared as broad peaks, and the reflections corresponding to the (111) and (200) planes seem to overlap with that of graphite at 26º. Its wideness indicates that better ceria dispersion was achieved on this sample. Finally it can be observed that the diffraction peak of graphite at 26º is sharper for samples Ni/G and Ni-CeO_2/G which indicates that these materials recovered the graphitic structure to a higher extent, this being in agreement with TEM images showing thicker layers on these samples.

The Raman spectra of graphite, GO, and the calcined catalysts are shown in Fig. 3. The spectrum of graphite is characterized by two main bands, D (1325 cm^{-1}) and G (1576 cm^{-1}), which are ascribed to the vibration of carbon atoms in disordered or defect sites and in-phase vibration of sp^2-bonded carbon atoms, respectively[26]. Therefore, the intensity ratio of the two bands (I_D/I_G) may be taken as an indication of the average size of sp^2 domains; it is reported as insert in Fig. 3. For GO it can be observed that the D and G bands are much more intense and wider compared to those in graphite, and the maxima were shifted to 1333 cm^{-1} and 1602 cm^{-1} respectively, indicating a higher level of disorder and defects. Moreover, the I_D/I_G ratio increased as a consequence of the reduction in the size

of the in-plane sp^2 domains. The catalysts displayed the D band at around the same frequency as GO; however, the G band was shifted to lower values (1576-1588 cm^{-1}), which can indicate that these materials have recovered the aromatic character to some extent. In addition, the spectra of the catalysts showed a new contribution as a shoulder at 1610 cm^{-1}, which corresponds to the D´-band. This band is due to modifications in the hexagonal ring tension caused by the arrangement of the electronic cloud; it increases with decreasing the order degree [27]. The I_D/I_G intensity ratio followed the order: graphite < Ni/G-Na < Ni/G < Ni-CeO_2/G-Na < Ni-CeO_2/G < GO. During the catalysts synthesis, the material partially recovered the aromatic structure but, the size of the layers decreased and the new materials contained more defects than graphite. The ceria-containing catalysts displayed a higher I_D/I_G ratio compared to Ni/G and Ni/G-Na, probably as a consequence of the incorporation of ceria, which creates more flaws, as previously suggested [19]. Furthermore, the typical peaks of the F2g vibration mode of ceria and the oxygen vacancies in the ceria lattice in the range 450-550 cm^{-1}were observed on sample Ni-CeO_2/G-Na (Fig. S2) [19,28].

Fig. 4 shows the evolution of H_2 consumption as a function of temperature for the calcined catalysts (He, 623 K, 5h) in H_2-TPR experiments. In addition to the m/z =2 signal (H_2), the m/z = 18, 28, 44, and 16 signals, which correspond to the main fragmentation patterns of H_2O, CO, CO_2 and CH_4, were also followed by on line mass spectrometry. It was observed that m/z = 18 was the major contribution to the profile, this confirming that the reduction of nickel oxide and cerium oxide were the main processes during the experiments. The H_2-TPR profile (H_2 consumption) of Ni/G-Na and Ni/G (Fig. 4a) showed broad bands with maxima at 692 K and 640 K respectively, assigned to the reduction of NiO nanoparticles.

The wideness of these bands points to the presence of NiO nanoparticles with different reducibility, especially for Ni/G, which could be due to the existence of particles with different interaction with the carbon support. The profiles changed after addition of ceria and, now, three distinguishable peaks could be seen for Ni-CeO_2/G-Na with maxima at 578, 626 and 801 K. On the other hand, the reduction profile for Ni-CeO_2/G showed two broad bands with maxima at 573 and 873 K. Reduction of bulk NiO and CeO_2 has been reported at 637 K [29] and 1123 K [30] respectively. When these oxides are supported their reducibility varies and a shift to lower reduction temperatures is expected. While for the ceria-free catalysts the H_2 consumption is mainly due to the reduction of NiO, no unambiguous assignation can be done for samples Ni-CeO_2/G-Na and Ni-CeO_2/G, where the reduction of NiO and CeO_2 might be overlapped especially in catalyst Ni-CeO_2/G. The H_2 consumption due to the reduction of the remaining oxygen groups on the support cannot be excluded, but this would represent a low percentage of the overall profile. Considering the H_2-TPR profile for Ni/CeO_2 and previous results [31], the low temperature peak can be ascribed to the reduction of NiO nanoparticles, and the peak at higher temperature could be due to the reduction of surface ceria. In general, the reduction temperatures are relatively high compared to other systems in which Ni and CeO_2 were supported over activated carbon [32]. This can be likely due to the stronger nanoparticles-support interaction achieved as a consequence of the presence of oxygen groups on the surface of the GO. In addition, as the TEM images showed, the incorporation of ceria in the sample Ni-CeO_2/G-Na afforded smaller NiO nanoparticles than those observed in the ceria-free catalyst, this leading to a lower reduction temperature. The effect of ceria addition has been reported for other

nickel catalysts, as Ni/SBA-15, where a decrease of the reduction temperature was also observed [33]. Furthermore, the presence of sodium in Ni-CeO_2/G-Na, which is confirmed by XPS (see below), could promote the formation of oxygen vacancies on the ceria surface, and this would be responsible for the lower temperature at which NiO reduction takes place in this catalyst [34].

The infrared spectrum of GO, (Fig. S3), showed the characteristic bands at 3387, 1719, 1224 and 1052 cm-1 ascribed to the stretching vibration of O-H, C=O, C-OH and C-O, respectively [12,35]. Although a peak at 1579 cm^{-1} corresponding to the skeletal vibrations of non-oxidized graphitic domains was observed, the spectrum confirms the successful oxidation of graphite. The spectra of the reduced catalysts showed a marked decrease of the band at 1719 cm^{-1} as well as some differences in the low frequency region, this confirming the partial reduction of GO.

Analyses of the XPS spectra of GO and the reduced catalysts were performed. The relative amounts of the different species were calculated from the corresponding peak areas taking into account the sensitivity factors, and the most relevant data are shown in Table 1. It can be observed that the Ni/C and Ce/C ratios for the Na-containing catalysts are higher, which is indicative of a higher dispersion of these species on the catalyst surface, in agreement with TEM results.

The position of the maximum for the C 1s spectrum of GO (Fig. S4) at 286.0 eV and the absence of the $\pi \rightarrow \pi^*$ peak characteristic of large poly-aromatic structures, indicated that the main contribution is assigned to sp^3 carbon, as expected [12]. The C 1s bands of the reduced catalysts were shifted to lower BE (284.6 eV), which indicates the partial recovery of the aromatic character, as the

Raman spectra suggested. The O 1s region of GO in Fig. 5 showed the contribution of three components: carbonyl oxygen (peak A, 531.4 eV), oxygen atoms in C-O bonds like hydroxyl and ether groups (peak B, 532.6 eV) and oxygen atoms in acidic carboxyl groups (peak C, 534.6 eV). This region is somewhat different for the catalysts, and the bands can now be deconvoluted into three main components: peak A, at 529.4-529.8 eV, peak B at 531.1-531.6 eV and peak C at 533.0-533.4 eV. Considering the infrared spectra and the absence of any peak on the N 1s region, a tentative assignation of the peaks according to literature can be as follows. Peak A would be ascribed to oxygen in CeO_2 and/or NiO[36,37]; peak B, to defective oxygen as oxygen atoms in the vicinity of Ni and Ce vacancies [38], although it might also include the contribution of the ceria hydroxyls and remaining oxygen groups [39], and peak C to oxygen in bridge-type Ce-O-Na or Ni-O-Na [35], although it could also include the contribution of adsorbed water [40].

The Ni $2p_{3/2}$ region of the different catalysts showed two main contributions at 854.2-856.0 and 856.0-857.6 eV, in contrast to the lower values at which these components are observed for Ni/CeO_2, as shown in Table 2. The contributions observed for the reduced catalysts at low and high binding energies have been ascribed to Ni^0 and NiO or $Ni(OH)_2$ respectively [30,41], which would be in quite good agreement with the H_2-TPR results. The reduction profile showed that under the reduction conditions employed only a small fraction of nickel could be reduced, although this fraction has not been detected by XPS. The binding energies of nickel species in the ceria-containing catalysts are shifted to higher values than the values reported for the pure compounds, this being an indication of their interaction with ceria. Furthermore, these values are higher for the

sodium-containing samples, this indicating that there is also an interaction between Ni species and the sodium promoter. All these interactions can modify the structure and electronic properties of Ni, which could improve the catalytic behaviour of this system[36].

The XPS analysis of the Ce 3d region indicated that both Ce^{4+} and Ce^{3+} were present in the catalysts surface, as the characteristic multiplets of $3d_{5/2}$ and $3d_{3/2}$ core holes were observed. The spectra were therefore deconvoluted into 10 peaks corresponding to Ce^{+4} and Ce^{+3} species [33]and the binding energies are shown in the supporting information (Table S1). The surface relative amount of Ce^{+3} was estimated, and the values are reported in Table 1. It can be observed that the contribution of Ce^{+3} to the overall spectra followed the trend Ni-CeO_2/G-Na > Ni/CeO_2 > Ni-CeO_2/G. Finally, the Na 1s region for samples Ni-CeO_2/G-Na and Ni/G-Na displayed one contribution at 1071.5-1071.6 eV, which is between the values reported for metallic Na and Na_2O or NaOH [42] and, considering the results obtained for the O 1s and Ce 3d regions, it might be ascribed to sodium interacting with Ce and Ni forming Na-O-Ce and Na-O-Ni species.

In conclusion, the binding energies of Ni and Ce species are shifted to higher values than those reported for Ni/CeO_2/activated carbon systems, and this seems to indicate a higher interaction between the Ni nanoparticles and the support, as also the H_2-TPR results suggested [32].

3.2 Reaction

Fig. 6 reports the catalytic activity results of the different samples in the low temperature WGS reaction, in terms of CO conversion as a function of temperature. Activity at each temperature has been determined after 2 h

stabilization, and no deactivation was detected during this period. It can be observed that Ni/G-Na, Ni-CeO_2/G-Na and Ni-CeO_2/G were active to different extents under the reaction conditions used, and the selectivity to CO_2 was 100% in the whole range of temperatures. The activity obtained with Ni-CeO_2/G-Na was only slightly lower than that achieved with the catalyst prepared over massive ceria (Ni/CeO_2), and the maximum CO conversions at 553 K was 94%, 84%, 34% and 7% for Ni/CeO_2, Ni-CeO_2/G-Na, Ni/G-Na and Ni-CeO_2/G respectively. The reaction results showed the fundamental role of ceria and also the importance of the presence of Na, which is able to improve the catalyst activity in agreement with recent results obtained for Ni/Na/CeO_2, Pt/Na/Carbon nanotubes and Ru/alkali/carbon materials [38,43,44] based on experimental and theoretical calculations for Pt/SiO_2 and Pt/Al_2O_3 catalysts doped with alkali ions [45].

In the literature, two reaction mechanisms have been mainly proposed for this reaction over ceria-containing catalysts. The redox mechanism suggests that the ceria redox process assists the oxidation of CO to CO_2 and the reduction of H_2O to H_2[5]. The associative mechanism proposes that water is dissociated to hydroxyls on the oxygen vacancies on the ceria surface, and the formed hydroxyls react with CO adsorbed on the metal particles to yield formates, which decompose to CO_2 and hydrogen [46]. Furthermore, it has been also proposed, although mainly for Cu-based catalysts and higher reaction temperatures, that the reaction intermediate is a carboxyl which would further decompose into CO_2 and H_2[47].

Therefore, independently of the reaction mechanism, small CeO_2 particles are beneficial, as they will hold a higher proportion of defects and, thus, a higher number of oxygen vacancies, which is directly related to the catalytic activity.

The incorporation of cations with a valence state lower than +4 in the ceria support may improve the activity in several ways. On one hand, the new cations can displace Ce^{+4} in the lattice generating more oxygen vacancies and improving the reducibility of the catalysts, but they can also stabilize supported active nanoparticles avoiding their sintering [48,49,50]. The XPS results seem to indicate that for Ni-CeO_2/G-Na, sodium was incorporated in the lattice and not merely on the surface, which would be detrimental for the reaction [5]. The incorporation of Na^+ in the lattice also led to an easier reducibility of CeO_2, as observed by H_2-TPR, compared to Ni-CeO_2-G/. Moreover, the oxygen vacancies can be accounted for by the $Ce^{+3}/(Ce^{+3}+Ce^{+4})$ ratio estimated by XPS and reported in Table 2. The values clearly show that this ratio is higher for Ni-CeO_2/G-Na compared to Ni-CeO_2/G. On the other hand, it has been suggested that Pt-O-Na clusters might favour the dissociation of H_2O molecules and, according to the associative mechanism, improve the reaction rate [41,46]. Nonetheless, the activity obtained with Ni-CeO_2/G was lower than expected. According to its H_2-TPR profile, it displayed the maximum of H_2 consumption at much higher temperature than Ni-CeO_2/G-Na, which would be due to the stronger interaction of ceria with the carbon support. The higher temperature needed for the reduction of ceria would hinder the WGS reaction. Other reasons for the lower activity of Ni-CeO_2/G, as the presence of residual oxygen groups or the encapsulation of a certain proportion of the nanoparticles during the synthesis, cannot be excluded. In fact, the encapsulation of the nanoparticles would explain

the lower Ni and Ce surface content obtained by XPS that this sample displayed, and the different reducibility behaviour as the reduction of the nanoparticles would be hindered. As long as the ceria-free catalysts are concerned, it is interesting to note that Ni/G-Na was active even in the absence of CeO_2. It has been proposed that the reaction mechanism over Ni is similar to that for copper, and follows an associative mechanism analogous to that proposed for ceria [14,51,52,53] in which water is dissociated on the oxidized Ni surface to produce adsorbed hydroxyl groups and atomic hydrogen. The hydroxyl groups would then react with adsorbed carbon monoxide to form an intermediate and eventually decomposes into carbon dioxide and hydrogen. As it has been stated before, the presence of Ni-O-Na entities may favour the dissociation of water and thus, this reaction mechanism.

Therefore, according to the characterization and the reaction results, it has been corroborated the important role of sodium in improving the activity for WGS reaction. Considering the results it seems plausible to assume that an associative mechanism dictates the reaction on the studied systems. Moreover, it is important to highlight that, despite the low amount of ceria on the Ni-CeO_2/G-Na catalyst, the obtained conversion was close to that observed for Ni supported over massive ceria, and taking into account the different percentage of ceria, it is clear that the overall activity has been greatly enhanced.

4. Conclusions

We have developed Ni- and Ni-CeO_2 supported catalysts employing graphite oxide as starting support material and urea or sodium hydroxide as precipitating agents, and we have determined their catalytic activity in the WGS reaction. Interestingly, different dispersions of the active phases on the support were

obtained depending on the precipitating agent and the presence or absence of ceria. Thus, a highly homogeneous dispersion of nanoparticles was obtained for Ni/G and Ni-CeO_2/G-Na, whereas large nanoparticles and even agglomerations were observed for Ni/G-Na and Ni-CeO_2/G. This is reflected in the TPR results, as samples with smaller particles showed the reduction processes at lower temperatures. In any case, the TPR profiles of these samples were very different to that of a Ni/CeO_2 catalyst, for which the reduction peaks were much more defined, and this could indicate that an interaction exists between ceria and the graphene support which hinders the reducibility of the former. XPS characterization showed that nickel was in an oxidized state in the reduced catalysts, and that the binding energies of the samples prepared by precipitation with NaOH where higher than those prepared by precipitationwith urea. XPS analysis allowed to detect the presence of sodium in the catalysts when NaOH was used, and that this residual sodium was interacting with both nickel species and the ceria promoter.

Concerning the catalytic performance, we observed that the presence of sodium largely improved the catalytic activity in WGS when ceria was present. The positive effect of sodium can be explained considering its incorporation into the ceria lattice, this creating more oxygen vacancies, and improving the reducibility of the catalysts Moreover, the sodium-containing ceria-free Ni/G-Na catalyst was active, this offering the possibility of developing an active catalysts for WGS without CeO_2. It seems that the presence of Ni-O-Na entities can favor the dissociation of adsorbed water, which is also a factor the can enhance the catalytic activity.

Finally, the high concentration of oxygen on the parent support (GO) seems to create strong metal-support interactions, which may be detrimental for the reaction following a redox mechanism. This could explain the low activity obtained with the Ni/G/CeO_2 catalyst. However, further work would be required to understand the effect of the remaining oxygen groups on the support and of the synthesis conditions, with the aim of optimizing the preparation of these complex catalytic systems.

Acknowledgements

Authors thank to CONICYT (Chile, Postdoc FONDECYT 3130483) andMinisterio de Economía y Competitividad (Spain, MAT2010-21147 and MAT2013-45008-P) for financial support.

5. References

[1] K. O. Hinrichsen, K. Kochloefl, M. Muhler, in Handbook of Heterogeneous Catalysis (Wiley, 2008), vol. 8 pp. 2905-2920.

[2] T.R. Reina, S. Ivanova, V. Idakiew, J.J. Delgado, I. Ivanov, T. Tabakova, M.A. Centeno, J.A. Odriozola, Catal. Sci. Technol. 3 (2013) 779-787.

[3] G. Jacobs, L. Williams, U. Graham, G.A. Thomas, D.E. Sparks, B.H. Davis, Appl. Catal., A: Gen. 252 (2003) 107–118.

[4] J. Goscianska, M. Ziolek, E. Gibson, M. Daturi, Appl. Catal.B: Env., 97 (2010) 49-56.

[5] T. Shido, Y. Iwasawa, J. Catal,141 (1993) 71-81.

[6] A.M. Duarte de Farias, D. Nguyen-Thanh,M.A. Fraga. Appl. Catal. B: Env.93 (2010) 250-258.

[7] R. Buitrago, J. Ruiz-Martínez, J. Silvestre-Albero, A. Sepúlveda-Escribano, F. Rodríguez-Reinoso, Catal. Today 180 (2012) 19-24.

[8] Z.Li, L. Mo, Y.Kathiraser, S.Kawi, ACS Catal.4 (2014) 1526−1536.

[9]U. Oemar, M.L. Ang, W.F. Hee, K. Hidajat, S. Kawi, Appl. Catal. B: Env. 148–149 (2014) 231–242

[10] Y. Li, Q. Fu, M. Flytzani-Stephanopoulos, Appl. Catal. B: Env. 27 (2000) 179-191.

[11] S.H. Kim, S.W. Nam, H.I. Lee, Appl. Catal. B: Env. 81 (2008) 97–104.

[12] A.B. Dongil, B. Bachiller-Baeza, A. Guerrero-Ruiz, I. Rodríguez-Ramos, J. Catal. 282 (2011) 299–309.

[13] D.R. Dreyer, H-P.Jia, C. W. Bielawski,Angew.Chem. Int. Ed. 49 (2010) 6813–6816.

[14]M. Mirza-Aghayan, R. Boukherroub, M. Nemati, M. Rahimifard, Tetrahedron Lett.53 (2012) 2473–2475.

[15] K. Gotoh, T. Kinumoto, E. Fujii, A.Yamamoto, H. Hashimoto, T. Ohkubo, A. Itadani, Y. Kuroda, H. Ishida, Carbon, 49 (2011) 1118–1125.

[16] E. López-Guerra, A.M. Shanmugharaj, W.S. Choi,SungHunRyu, Appl. Catal. A: Gen.468 (2013) 467– 474.

[17] C. C. Yeh, D. Hwang Chen, Appl. Catal. B: Env.150– 151 (2014) 298–304.

[18] T. Niu, G.L. Liu, Y. Liu, Appl. Catal.B: Env. 154–155 (2014) 82–92.

[19] Z.Ji, X. Shen, J.Yang, G. Zhu, K. Chen, Appl. Catal. B: Env.144 (2014) 454-461.

[20] Y. Zhao, H.Zhang, C.Huang, S. Chen, Z. Liu, J. Coll. Interf. Sci. 374 (2012) 83–88.

[21] B.F. Machado, P. Serp, Catal. Sci. Technol. 2 (2012) 54-75.

[22] O. Mabayoje, M. Seredych and T. J. Bandosz, Appl. Catal. B: Env.132–133 (2013) 321– 331.

[23] D.C. Marcano, D.V. Kosynkin, J.M. Berlin, A. Sinitskii, Z.Sun, A. Slesarev, L.B. Alemany, W. Lu, J. M. Tour, ACS Nano4 (2010) 4806-4814.

[24] S.You, S. M. Luzan, T. Szabó, A.V. Talyzin, Carbon, 52 (2013) 171 –180.

[25] A.B. Bourlinos, D. Gournis, D. Petridis, T. Szabo, A. Szeri, I. Dekany, 19 (2003) 6050-6055.

[26] N. Larouche, B. L. Stansfield, Carbon, 48 (2010) 620–629.

[27] A. Cuesta, P. Dhamelincourt, V. Laureyns, A. Martínez-Alonso, J. M. D. Tascón, 32 (1994) 1523-1532.

[28] L. Katta, P. Sudarsanam, G. Thrimurthulu, B. M. Reddy, Appl. Catal. B: Env. 101 (2010) 101–108.

[29] R. Buitrago-Sierra, J. Ruiz-Martínez, J.C. Serrano-Ruiz, F. Rodríguez-Reinoso, A. Sepúlveda-Escribano, J. Coll. Interf. Sci. 383 (2012) 148–154.

[30] V. M. Shinde, G. Madras, Appl. Catal. B: Env. 132-133 (2013) 28-38.

[31] K. Chayakul, T. Srithanratana, S. Hengrasmee, Catal.Today 175 (2011) 420–429.

[32] L. Pastor-Pérez, R. Buitrago-Sierra, A. Sepúlveda-Escribano, Int. J. Hyd. Energy, 39 (2014) 17589-17599.

[33] I. Jiménez-Morales, F. Vila, R. Marisca, A. Jiménez-López, Appl. Catal. B: Env. 117-118 (2012) 253-259.

[34] B. Zugic, D. C. Bell, M. Flytzani-Stephanopoulos, Appl. Catal. B: Env. 144 (2014) 243-251.

[35] T. Szabó, O. Berkesi, P. Forgó, K. Josepovits, Y. Sanakis, D. Petridis, I. Dékány, Chem. Mater. 18 (2006) 2740-2749.

[36] S. Velu, K. Suzuki, M. Vijayaraj, S. Barman, C.S. Gopinath¸ Appl. Catal. B: Env. 55 (2005) 287–299.

[37] J. Światowska, V. Lair, C. Pereira-Nabais, G. Cote, P. Marcus, A. Chagnes, Appl. Surf. Sci. 257 (2011) 9110– 9119.

[38] D. Andreeva, P. Petrova, J.W. Sobczak, L. Ilieva, M. Abrashev, Appl. Catal. B: Env. 67 (2006) 237–245.

[39] A. Bensalem, F. Bozon-Verduraz, M. Delamar and G. Bugli, Appl. Catal. A: Gen. 121 (1995) 81-93.

[40] A.B. Dongil, B. Bachiller-Baeza, A. Guerrero-Ruiz, I. Rodríguez-Ramos, A. Martínez-Alonso, J. M. D. Tascón. J. Coll. Interf. Sci. 355 (2011) 179-189.

[41] J-H. Lin, V.V. Guliants, ChemCatChem 4 (2012) 1611-1621.

[42] H.W. Nesbitt, M. Bancroft, G.S. Henderson, R. Ho, K.N. Dalby, Y. Huang, Z. Yan, Thin Solid Films 531 (2013) 170-180.

[43] M.L. Ang, U. Oemar, E.T. Saw, L. Mo, Y. Kathiraser, B.H. Chia, S. Kawi, ACS Catal.4 (2014) 3237−3248.

[44] B. Liu, T. Huang, Z. Zhang, Z. Wang, Y. Zhang, J. Li, Catal. Sci. Technol. 4 (2014) 1286-1292.

[45] Y. Zhai, D. Pierre, R. Si, W. Deng, P. Ferrin, A.U. Nilekar, G. Peng, J.A. Herron, D.C. Bell, H. Saltsburg, M. Mavrikakis,M. Flytzani-Stephanopoulos, Science, 329 (2010) 1633-1636.

[46] D. Andreeva, V. Idakiev, T. Tabakova, A. Andreev, R. Giovanoli, J. Catal. 158 (1996) 354–355.

[47] E.T. Saw, U. Oemar, X.R. Tan, Y. Du, A. Borgna, K. Hidajat, S. Kawi, J.Catal. 314 (2014) 32–46.

[48] D. Andreeva, P. Petrova, J.W. Sobczak, L. Ilieva, M. Abrashev, Appl. Catal. B: Env. 67 (2006) 237-245.

[49] M. Yang, S. Li, Y. Wang, J.A. Herron, Y. Xu, L.F. Allard, S. Lee, J. Huang, M. Mavrikakis, M. Flytzani-Stephanopoulos, Science, 346 (2014) 1498-1501.

[50] B. Zugic, S. Zhang, D.C. Bell, F. Tao, M. Flytzani-Stephanopoulos, J. Am. Chem. Soc. 136 (2014) 3238-3245.

[51] M.S. Spencer, Catal. Today 12 (1992) 453-464.

[52] G.C. Chinchen, M.S. Spencer, J. Catal. 112 (1988) 325-327.

[53] Y. Li, Q. Fu, M. Flytzani-Stephanopoulos, Appl. Catal. B: Env. 27 (2000) 179-191.

Table 1. XPS surface atomic ratiosin the reduced catalysts.

Sample	O/C	Ce/C	Ni/C	Ni/Ce	Na/C	$Ce^{+3}/(Ce^{+3}+Ce^{+4})$
Ni/G	0.12	-	0.01	-	-	-
Ni-CeO_2/G	0.69	0.03	0.01	0.33	-	23
Ni/G-Na	0.19	-	0.02	-	0.10	-
Ni-CeO_2/G-Na	0.59	0.07	0.04	0.49	0.04	44
Ni/CeO_2	-	-	-	0.13	-	33

Table 2. Ni $2p_{3/2}$ and Na 1s binding energies of the reduced catalysts.

Catalysts	Ni $2p_{3/2}$ (eV)		Na 1s (eV)
	Ni^0	NiO /$Ni(OH)_2$	
Ni/G	-	854.2/856.0	-
Ni-CeO_2/G	-	854.4/856.4	-
Ni/G-Na	-	855.6/857.5	1071.6
Ni-CeO_2/G-Na	-	856.0/857.6	1071.5
Ni/CeO_2	852.3	854.3/856.5	-

Fig. 1. TEM micrographs of a) Ni/G-Na, b) Ni/G¸ c) Ni/G/CeO_2-Na,d) Ni/G/CeO_2, e) Ni/CeO_2, and particle size distributions of f) Ni/G-Na and g) Ni/G.

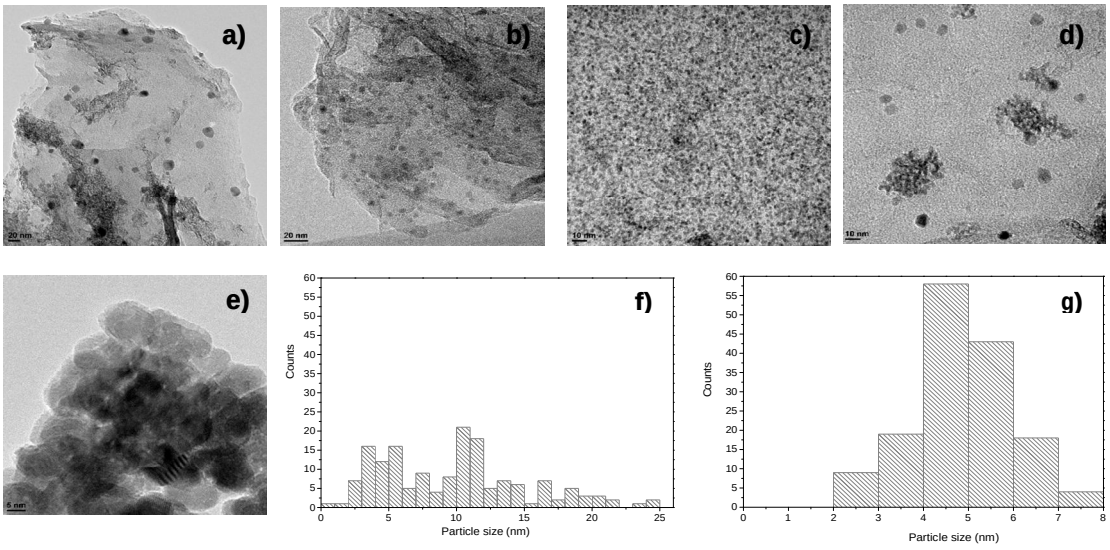

Fig. 2. X-ray diffraction patterns of graphite, graphite oxide and the calcined catalysts.

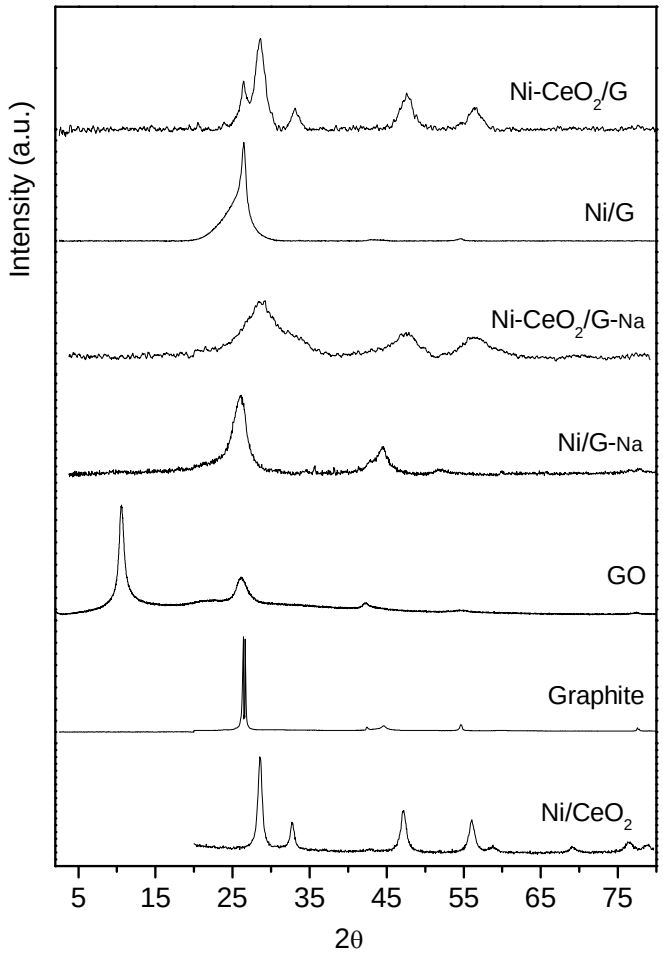

Fig. 3. Raman spectra of graphite, graphite oxide and the calcined catalysts.

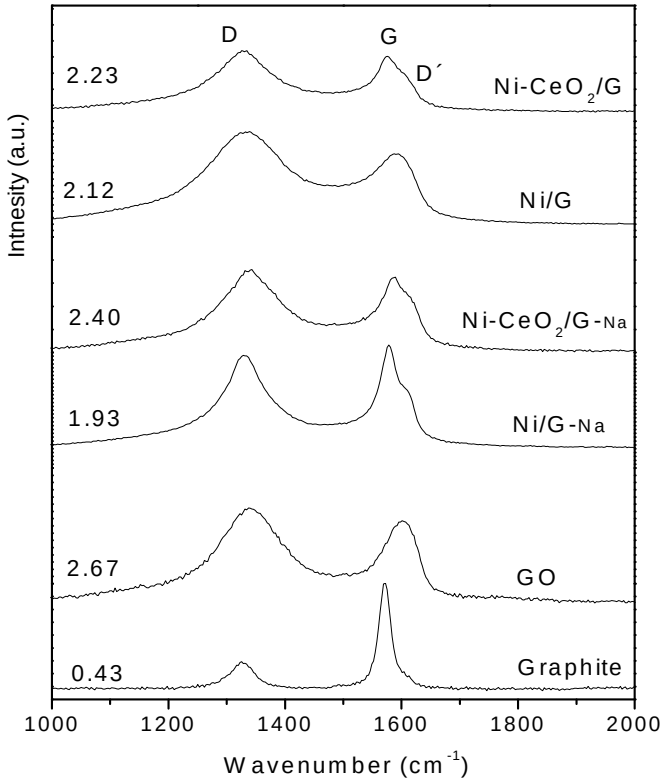

Fig. 4. H_2-TPR profiles of calcined catalysts: a) Ni/G (—), Ni/G-Na(---); b) Ni-CeO_2/G(—), Ni-CeO_2/G-Na (---) and, c) Ni/CeO_2.

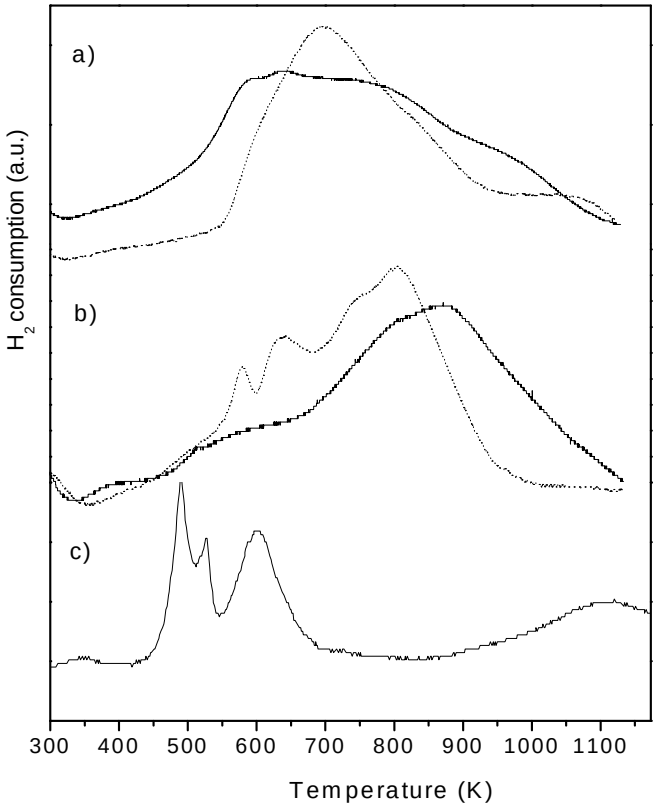

Fig. 5. Core level XP-spectra of the O 1s region for graphite oxide and the reduced catalysts.

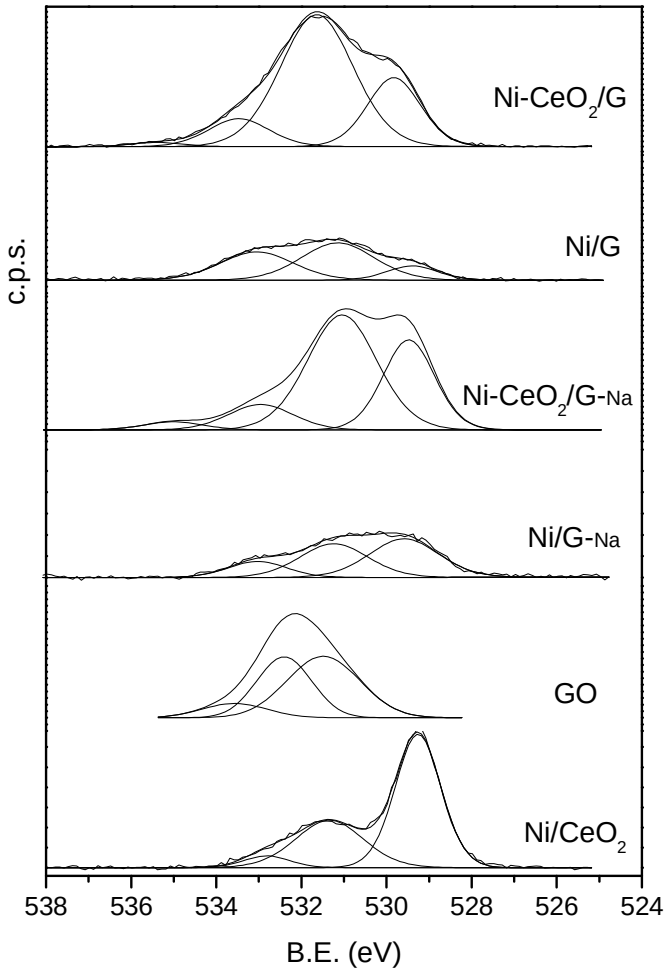

Fig. 6. CO conversion vs. reaction temperature in idealized feed (1.75% CO, 35.92% H_2O, and He balance), for catalysts reduced at 673 K.